Desalination and Water Treatment
www.deswater.com
doi: 10.1080/19443994.2013.814000

52 (2014) 4734–4744
July

Taylor & Francis
Taylor & Francis Group

On precipitated calcium and magnesium phosphates during synthetic hard waters softening by monosodium phosphate

A.S. Manzola[a,*], A. Mgaidi[b], M.S. Laouali[a], M. El Maaoui[b]

[a]*Laboratoire de Chimie Analytique et Minérale, Faculté des sciences, Université Abdou Moumouni, BP 10662 Niamey, Niger*
Tel. +227 20315072; Fax: +22720315862; email: abdoussalam_manzola@yahoo.com
[b]*Laboratoire de Chimie Minérale Industrielle, Faculté des sciences, Université de Tunis, El Manar, BP 37, El Belvédère 1002, Tunis, Tunisia*

Received 12 July 2012; Accepted 5 May 2013

ABSTRACT

Phosphates were largely used to soften process or drinking waters. We have investigated the precipitation of Ca^{2+} and Mg^{2+} ions by monosodium phosphate dehydrate. Magnesium phosphate starts precipitating at $pH_0 = 8.6$. The obtained solids have been identified by chemistry analyses, FTIR spectroscopy, X-ray diffraction, thermo gravimetric analysis and differential thermal analysis. The solid phases obtained vary with pH_0. It shows that DCPD (dicalcium phosphate dehydrate, $CaHPO_4{\cdot}2H_2O$) precipitated within pH_0 5 to 6.6, the TCP (tricalcic phosphate) and other apatite appear below $pH_0 = 7$. The DCPD (dicalcium phosphate dihydrate, $CaHPO_4{\cdot}2H_2O$,) precipitated was a pure product that can be used in nanotechnology and biomedical technology. We are presently testing these solids for natural waters defluoridation.

Keywords: Softening; Synthetic hard waters; Settling time; Calcium; Magnesium; Phosphates; Solid phases

1. Introduction

Hard water generates scaling in water distribution circuits, and it leads to the development of renal calculi and the calcification of the cardiovascular system. Phosphates were largely used to soften processed or drinking waters. Required French Standard with regard to phosphates for drinking waters after treatment is 5 mg/L P_2O_5 [1]. No indicative value is recommended by World Health Organisation [2]. Various methods of calcium phosphates precipitation from aqueous solutions were studied [3–5]. Investigations of the precipitation phenomenon in calcium phosphate solutions and the interactions between precipitated solid phases are importantly applied in industries for water treatment and biological mineralization [6,7]. The precipitation and dissolution of phosphates in aqueous systems, an important chemical process, occurs in industrial processes, in the mineralization of bone and in many other geochemical fields. Hydroxyapatite ($Ca_5(PO_4)_3OH$, HAP) and others biological apatites are the most important calcium phosphates precipitated. Elucidations of the mechanism of precipitation and the nature of the precipitated phases have considerable importance.

*Corresponding author.

The precipitation of HAP and other calcium phosphates were studied with seeded crystal growth methods using a variety of calcium phosphates as seed [8]. In solution, initially supersatured with respect to dicalcium phosphate dihydrate ($CaHPO_4{\cdot}2H_2O$, DCPD) and octacalcium phosphate ($Ca_8H(PO_4)_6{\cdot}5H_2O$, OCP), crystal growth on HAP seeds occurs with the formation of precursor phases, usually OCP [9]. A number of calcium phosphate phases such as amorphous calcium phosphate (ACP), dicalcium phosphate dihydrate ($CaHPO_4{\cdot}2H_2O$, DCPD) and octacalcium phosphate [Ca_8H $(PO_4)_6{\cdot}5H_2O$, OCP] were proposed as precursors to obtained the most stable thermo dynamical phase or HAP ($Ca_5(PO_4)_3OH$, HAP), under physiological conditions [10]. In neutral and acidic solutions, DCPD was found to be the first crystalline phase to precipitate with the additional possibility of the formation of an unstable amorphous phase as a precursor [11,12]. Although the formation of DCPD at physiological pH 7.4 is expected to precede that of OCP [13], it is therefore of interest to study the development of more basic calcium phosphate phases in the DCPD suspensions. The transformation phase from DCPD to OCP and subsequently to more basic phases was previously investigated using a potentiostatic method at pH values maintained by automated addition of base [14,15]. Thus, it has been shown that the nature of the calcium phosphate phase formed during precipitation from aqueous solutions is markedly dependent on the calcium and phosphate concentrations, pH and the nature and extent of the surface phases on which precipitation occurs [16,17]. In light of that, the nature of the precipitating phase depends not only on the pH but also on the supersaturation, and so, it is important to study the kinetics transformation phase at constant solution composition. Calcium phosphates are used as biomaterial for hard tissues repair. Cracks responsible of teeth enamel pain can be filled ten times more rapidly with calcium phosphates nanoparticles (apatite). Calcium phosphate simulates the tooth natural matter and fills enamel cracks. The composite rematerialized layer acts as a natural one. For these new properties obtainable at nanoscale, calcium phosphate nanoparticles have been prepared. Calcium phosphate nanoparticles were obtained by HAP target by laser ablation technique in water and in ambient conditions, also by Pulsed laser ablation technique of synthetic hydroxyapatite target with a pulsed CO_2 laser. The technique of laser ablation of solids in liquids has been used to obtain colloidal nanoparticles from biological hydroxyl apatite using pulsed as well as a continuous wave laser [18,19]. Phosphates of magnesium frequently obtained are trimagnesium hydrated phosphates, very difficult to obtain because of their thermal instability, recently obtained from bobierrite $Mg_3(PO_4)_2{\cdot}8H_2O$ [16,17]. $Mg_3(PO_4)_2{\cdot}22H_2O$ prepared at pH 9. Struvite $Mg(NH_4)(PO_4){\cdot}6H_2O$ and Whitlockite $Ca_{18}(Mg_2)H_2(PO_4)_{14}$ [20]. Struvite precipitates were obtained at pH ranging between 7 and 11 in which phosphorus, magnesium and the ammonia were found at ambient temperature. In our experimental conditions, we cannot obtain struvite as we did not have ammonia in our solution.

The paper investigated precipitated calcium and magnesium phosphates during synthetic hard waters softening by monosodium phosphate at pH values varying from 5.8 to 8.6, and the influence of initial Ca, Mg and PO_4 concentrations. The purpose was to determine the effects of these factors (pH, concentrations) on crystal growth and morphology of precipitated calcium and magnesium phosphates, but also their effects on solids co-existence and transformation into other types of calcium and magnesium phosphates. Synthetic solutions obtained by dissolution of magnesium and calcium chlorides in distilled water were studied.

2. Experimental setup and procedures

2.1. Ca^{2+} synthesized water

Synthesized water was prepared by dissolving 3.225 g of $CaCl_2.H_2O$ in a litre of distilled water. The solution obtained is 1 g/L of Ca^{2+} ions.

2.2. Mg^{2+} synthesized water

Synthesized water was prepared by dissolving 4.18 g of $MgCl_2.6H_2O$ in a litre of distilled water and the solution obtained is 0.5 g/L of Mg^{2+} ions.

2.3. Precipitation reagent

Precipitation reagent was prepared by dissolving 12 g of $NaH_2PO_4{\cdot}2H_2O$ in a litre of distilled water, the solution obtained was 0.0769 mol/L of H_2PO_{4-} ions. In 100 ml of synthesized water contained in a tricol balloon were added variable volumes of precipitation reagent. The calcium phosphate precipitation was controlled by pH adjustment with 1 M NaOH solution using a pH-meter Tacussel giving an accuracy of 0.01 unit of pH. The medium agitation was carried out using a magnetic stick at an ambient temperature between 22 and 25°C. The precipitated solution was poured in a 250 ml bottle and kept for 1, 3 or 7 days, then filtered. The precipitated solid was dried between 60 and 70°C for 24 h.

The solid phases obtained at different pH_0 were characterized, by powder X-ray diffraction and phase identification was made using an ASTM card [21], and chemical analysis (The Ca was analysed by EDTA titration, Mg was analysed using atomic absorption spectrophotometer (AAS) Perkin Elmer, P was analysed by vanadomolybdo phosphoric acid colorimetric method). To determine the dehydration temperature and the amount of water in the precipitated solids occurring both as surface physisorbed water and water coordinated to the solid phases, a thermo gravimetric analysis (TGA) was meticulously done at different temperatures, and using an analytical balance, we measured the weight loss of the material. To determine the allotropic phase transformation of precipitated solids, differential thermal analysis (DTA) was undertaken at different temperature. This study is only centred on solids precipitated with the addition of 2 g of phosphate, filtered after one day and then characterized.

3. Results and discussion

3.1. Experimental results

We investigated the effect of initial pH on the nature of solid precipitated calcium phosphate phases.

3.1.1. Calculation of Ca/P ratio by chemical analysis of precipitated solids

Considering the evolution of the precipitated solids according to the pH value, we made eight comparison tests with $pH_0 = 5.8$, 6.2, 6.6, 7, 7.4, 7.8, 8.2, and 8.6. Table 1 gives the chemical analysis of the precipitated solids.

Precipitated solids Ca/P ratio values for $pH_0 = 5.8$, 6.2 and 6.6 are close to 1. Ca/P ratio values for $pH_0 = 7$, 7.4, 7.8, 8.2 and 8.6 are on average 1.44.

Table 1
Calculation of the molar Ca/P ratio of the precipitated solids according to the pH_0

pH_0	% Ca (g/g)	% P (g/g)	Ca (mol)	P (mol)	Ca/P
5.8	19.73	16.86	0.49	0.54	0.91
6.2	19.62	16.49	0.49	0.53	0.92
6.6	19.53	16.75	0.49	0.54	0.91
7	30.24	16.95	0.76	0.54	1.41
7.4	29.96	16.36	0.749	0.52	1.44
7.8	29.92	16.12	0.748	0.52	1.44
8.2	29.86	16.01	0.72	0.51	1.46
8.6	29.90	16.10	0.747	0.52	1.44

3.1.2. Infra-red spectrometry

Considering the evolution of the precipitated solids according to the pH value, eight additional comparison tests were made with $pH_0 = 5.8$, 6.2, 6.6, 7, 7.4, 7.8, 8.2 and 8.6. The infra-red spectra of the precipitated solids at different pH_0 values are represented in Fig. 1.

Two kinds of spectra forms were observed:

The first form		The second form	
(a) ⟶	$pH_0 = 5.8$	(d) ⟶	$pH_0 = 7.0$
(b) ⟶	$pH_0 = 6.2$	(e) ⟶	$pH_0 = 7.4$
(c) ⟶	$pH_0 = 6.6$	(f) ⟶	$pH_0 = 7.8$, 8.2, 8.6

3.1.3. X-ray diffraction

Considering the evolution of the precipitatwed solids according to the pH value, we made eight comparison tests with $pH_0 = 5.8$, 6.2, 6.6, 7, 7.4, 7.8, 8.2 and 8.6. The X-ray diffraction diagrams of the precipitated solids at different pH_0 values are represented in Figs. 2 and 3.

3.1.4. TGA and DTA

Considering the evolution of the precipitated solids according to the pH value, we made eight comparison tests with $pH_0 = 5.8$, 6.2, 6.6, 7, 7.4, 7.8, 8.2, and 8.6. The TGA and DTA of the precipitated solids at $pH_0 = 6.2$, 7.8 are represented in Figs. 4 and 5. The samples were heated to 600°C under air flow.

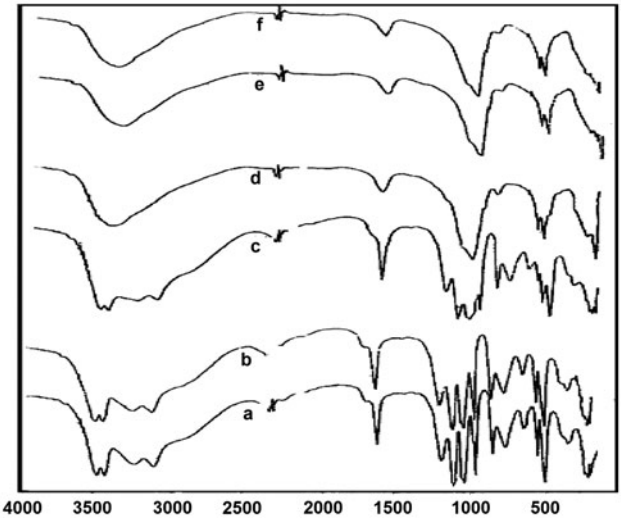

Fig. 1. Infra-red spectra of the precipitated solids at different pH_0.

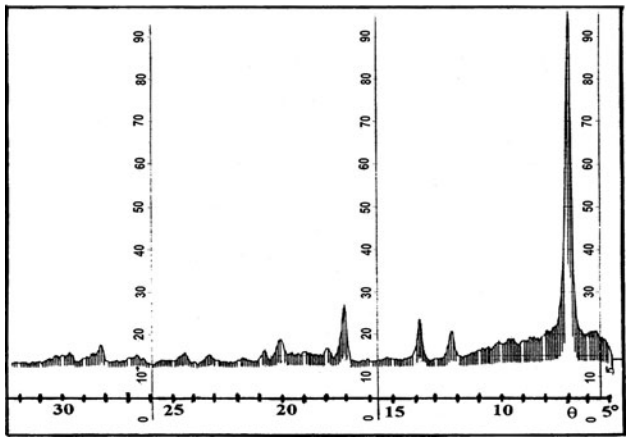

Fig. 2. Diagram of X-ray diffraction of the precipitated solid at $pH_0 = 6.2$.

3.1.5. Solubility product

Considering the evolution of the precipitated solids according to the pH value, we made 11 comparison tests with $pH_0 = 4.45$, 5.0, 5.4, 5.8, 6.2, 6.6, 7, 7.4, 7.8, 8.2, and 8.6. Table 2 gives the solubility products (Ks) of the precipitated solids from $pH_0 = 4.45$ to 6.6. Table 3 gives the solubility products of the precipitated solids from $pH_0 = 7$ to 8.6. The pH obtained after one day of settling was noted pH_f.

Solubility product of precipitated solids with $pH_0 = 4.45$, 5, 5.4, 5.8, 6.2, 6.6 and taken at pH_f 4.45, 4.6, 4.7, 4.94, 5.66, and 6.09 was calculated in accordance with Ca^{2+} and P_2O_5 concentrations (Table 2).

In this range of pH, the precipitated solid formula was supposed to be $CaHPO_4 \cdot 2H_2O$. Solutions equated with the precipitated product as shown by the following formula:

$$Ks = [Ca^{2+}][HPO_4^{2-}]$$

where $[Ca^{2+}]$ was directly determined from the solution and $[HPO_4^{2-}]$ determined by the following procedure:

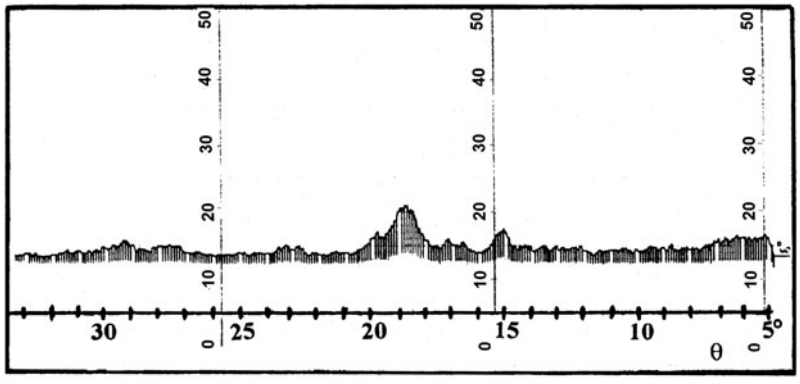

Fig. 3. Diagram of X-ray diffraction of the precipitated solid at $pH_0 = 7.8$.

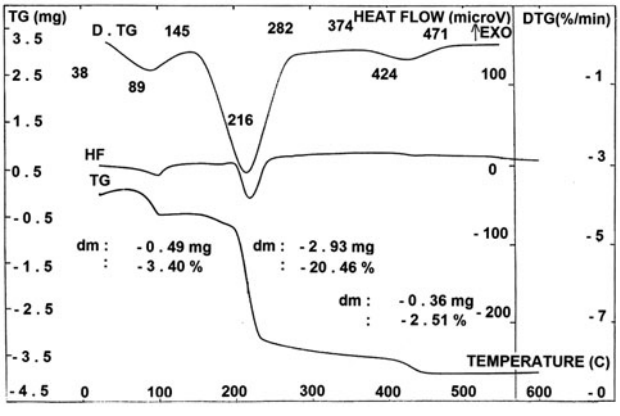

Fig. 4. Curves of TGA and DTA of the precipitated solid at $pH_0 = 6.2$.

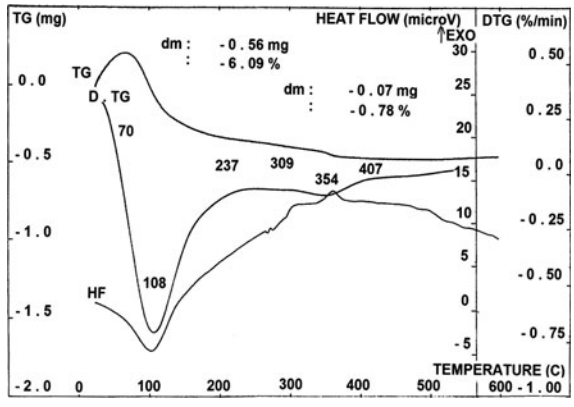

Fig. 5. Curves of TGA and DTA of the precipitated solid at $pH_0 = 7.8$.

Table 2
Solubility products of the precipitated calcium phosphate solids from pH_0 4.45 to 6.6

pH_0	pH_f	$[Ca^{2+}]$ (mol/L)	$[HPO_4^{2-}]$ (mol/L)	Ks
4.45	4.45	0.0235	1.94×10^{-5}	No solid
5	4.6	0.0205	2.68×10^{-5}	5.49×10^{-7}
5.4	4.7	0.0205	3.21×10^{-5}	6.58×10^{-7}
5.8	4.94	0.017	4.58×10^{-5}	7.78×10^{-7}
6.2	5.66	0.011	8.17×10^{-5}	8.98×10^{-7}
6.6	6.09	0.007	13.49×10^{-5}	9.44×10^{-7}

Table 3
Solubility products of the precipitated calcium phosphate solids from pH_0 7 to 8.6

pH_0	pH_f	$[Ca^{2+}]$ (mol/L)	$[HPO_4^{2-}]$ (mol/L)	Ks
7	5.6	0.0065	5.10×10^{-10}	8.18×10^{-77}
7.4	5.65	0.006	4.70×10^{-10}	2.44×10^{-77}
7.8	5.93	0.006	3.10×10^{-10}	2.01×10^{-78}
8.2	6.04	0.0045	4.12×10^{-10}	8.36×10^{-79}
8.6	6.04	0.0045	5.14×10^{-10}	3.12×10^{-78}

$$H_3PO_4 \leftrightarrows H_2PO_4^- + H^+ \qquad K_1 \quad pK_1 = 2.1$$

$$H_2PO_4^- \leftrightarrows H_2PO_4^{2-} + H^+ \qquad K_2 \quad pK_2 = 7.2$$

$$K_2 = \frac{[HPO_4^{2-}][H^+]}{[H_2PO_4^-]}$$

The phosphate evolution was followed by analysing the P_2O_5. P_2O_5 measured concentration gave us $[H_xPO_4^{3-x}]_{total}$ according to:

$$[H_xPO_4^{3-x}]_{total} = 2[P_2O_5]$$

On the other hand we have:

$$[H_2PO_4^-] + [HPO_4^{2-}] = [H_xPO_4^{3-x}]_{total}$$

According to the equilibrium we have:

$$[H_2PO_4^-] = \frac{[HPO_4^{2-}][H^+]}{K_2}$$

therefore $\frac{[HPO_4^{2-}][H^+]}{K_2} + [HPO_4^{2-}] = [H_xPO_4^{3-x}]_{total}$.

As $[H^+]$ was determined from the pH_f, we obtained $[HPO_4^{2-}]$.

As we were interested by the equilibrium given by K_2, as in studied pH_0, only $H_2PO_4^-$ et HPO_4^{2-} subsisted according to the phosphated species repetition diagram. It was the same for the $[PO_4^{3-}]$ calculations given by the K_3 equilibrium, where only $[HPO_4^{2-}]$ and $[PO_4^{3-}]$ subsisted in the pH_0 considered for the second solid precipitation.

Solubility product of precipitated solids in pH_0 going from 7 to 8.6 was calculated in the same conditions as those of precipitated solids in pH_0 going from 4.45 to 6.6. Table 3 gives the solubility products of precipitated solids. As the precipitated solid formula was supposed to be $Ca_9(PO_4)_{6-x}(HPO_4)_x(OH)_x$ we can realize that the solubility product is equal to:

$$Ks = [Ca^{2+}]^9[PO_4^{3-}]^{5.6}[HPO_4^{2-}]^{0.4}[OH^-]^{0.4}$$

For $x = 0.4$ (this value was obtained with TGA and DTA).

With $[OH^-]$ calculated from the pH_f and the $K_e = [OH^-][H^+]$ and $[PO_4^{3-}]$ in the following procedure:

$$H_2PO_4^{2-} \rightleftharpoons PO_4^{3-} + H^+ \quad K_3 \qquad pK_3 = 12.4$$

With

$$K_3 = \frac{[PO_4^{3-}][H^+]}{[HPO_4^{2-}]}$$

The concentration of $[H_xPO_4^{3-x}]_{total}$ was deducted from that of P_2O_5 measured, on the other hand:

$$[HPO_4^{2-}] + [PO_4^{3-}] = [H_xPO_4^{3-x}]_{total}$$

According to the equilibrium we have:

$$[HPO_4^{2-}] = \frac{[PO_4^{3-}][H^+]}{K_3}$$

therefore $\frac{[PO_4^{3-}][H^+]}{K_3} + [PO_4^{3-}] = [H_xPO_4^{3-x}]_{total}$

As $[H^+]$ was determined from the pH_f we obtained $[PO_4^{3-}]$.

The exponents for Ks in Table 3 are correct, and were calculated according to:

$$Ks = [Ca^{2+}]^9[PO_4^{3-}]^{5.6}[HPO_4^{2-}]^{0.4}[OH^-]^{0.4}$$

as the precipitated solid formula was supposed to be $Ca_9(PO_4)_{6-x}(HPO_4)_x(OH)_x$ or in Table 2, they were calculated according to: $Ks = [Ca^{2+}][HPO_4^{2-}]$ as the precipitated solid formula was supposed to be $CaHPO_4{\cdot}2H_2O$.

The values of the solubility products of precipitated solids obtained in Table 2 are in conformity of

those obtained by Nancollas and Wefel [17], the solubility product of $CaHPO_4{\cdot}2H_2O$ at 5°C is of about $2.1 \pm 0.09 \times 10^{-7}$ mole^2 L^{-2}. The values of the solubility products of precipitated solids obtained in Table 3 are in conformity of those obtained by Sarubina [22] and Gregory [23], and of about 10^{-78} mole^2 L^{-2} for the lacunar apatite [22,23]. We can realize that all of these values are close to those obtained by Nancollas [16], Sarubina [22] and Gregory [23].

It is evident that there are considerable disproportions between Ks for $pH_0 = 6.6$ and 7.0, because at $pH_0 = 6.6$ the precipitated solid is $CaHPO_4 \cdot 2H_2O$ and at $pH_0 = 7.0$ the precipitated solid is $Ca_9(PO_4)_{5.6}(HPO_4)_{0.4}(OH)_{0.4}$.

Molle [24] defined precipitation as the accumulation of a substance developing a new solid tridimensional phase. According to him, the distribution of phosphated forms and therefore their precipitation is governed by the pH. Consequently, the solubility of the precipitate will be strongly controlled by the pH.

According to the equilibrium:

$$K_2 = \frac{[HPO_4^{2-}][H^+]}{[H_2PO_4^-]}$$

we have: $[H_2PO_4^-] = \frac{[HPO_4^{2-}][H^+]}{K_2}$

Tables 2 and 3 give the $[HPO_4^{2-}]$ at $pH_0 = 6.6$ and 7.0. At $pH_0 = 6.6$ $[H_2PO_4^-] = 173.77.10^{-5}$ mol/L and at $pH_0 = 7.0$ $[H_2PO_4^-] = 199.05.10^{-10}$ mol/L.

3.2. Magnesium precipitation—experimental results

3.2.1. Calculation of Mg/P ratio by chemical analysis of precipitated solids

Under our experimental conditions, magnesium starts precipitation at $pH_0 = 8.6$. A 100 ml batch of 500 mg/L Mg^{2+} solution was treated with variable amounts of added phosphate. The treated solution was kept for 1 or 3 days settling.

Table 4 gives the chemical analysis of the precipitated solids obtained when 12.8×10^{-3}, 15.4×10^{-3}, 17.8×10^{-3} and 19.9×10^{-3} mol/L of phosphate are added.

3.2.2. Infra-red spectrometry

The infra-red spectrum of the precipitated solids at $pH_0 = 8.6$ is represented in Fig. 6.

3.2.3. X-ray diffraction

The X-ray diffraction of the precipitated solids at $pH_0 = 8.6$ is represented on Fig. 7.

3.2.4. TGA and DTA

The TGA and DTA of the precipitated solids at $pH_0 = 8.6$ is represented in Fig. 8. The samples were heated up to 600°C under air flow.

3.3. Discussions

3.3.1. Calcium phosphates precipitation

3.3.1.1. Chemical analysis of precipitated solids—calculation of Ca/P ratio. For the chemical analysis of the solids, the Ca/P ratio values for $pH_0 = 5.8$, 6.2 and 6.6 are close to 1 which is the characteristic ratio value of $CaHPO_4$.

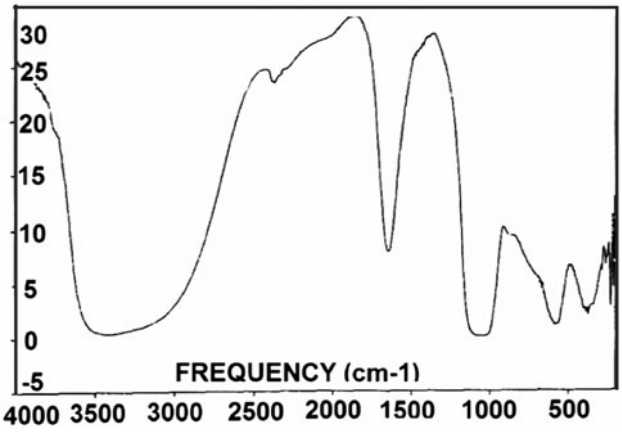

Fig. 6. Infra-red spectrum of the precipitated magnesium phosphate solid at $pH_0 = 8.6$.

Table 4
Calculation of the molar Mg/P ratio of the precipitated solid at pH_0 8.6

$[H_2PO_4^-]_{0added}$ (mol/L)	% Mg^{2+} (mg/mg)	% P_2O_5 (mg/mg)	Mg^{2+} (mol)	P_2O_5 (mol)	Mg/P (molar ratio)
12.8×10^{-3}	10.5	7	4.32×10^{-4}	0.49×10^{-4}	4.4
15.4×10^{-3}	10.5	7	4.32×10^{-4}	0.49×10^{-4}	4.4
17.8×10^{-3}	14.45	17	5.94×10^{-4}	1.19×10^{-4}	2.5
19.9×10^{-3}	7.49	1.7	3.08×10^{-4}	0.12×10^{-4}	12.8

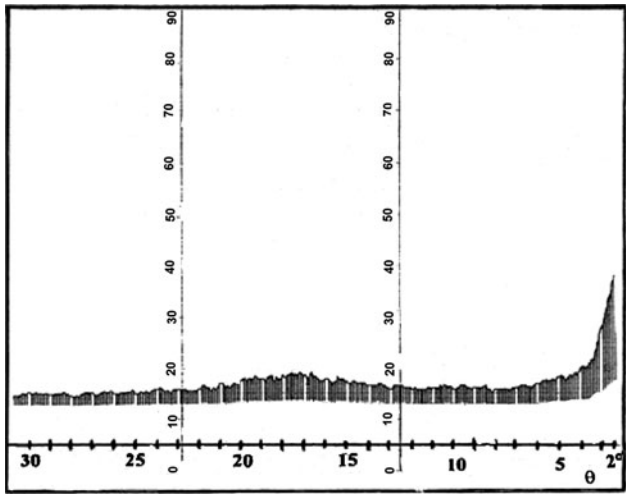

Fig. 7. Diagram of X-rays diffraction of the precipitated magnesium phosphate solid at $pH_0 = 8.6$.

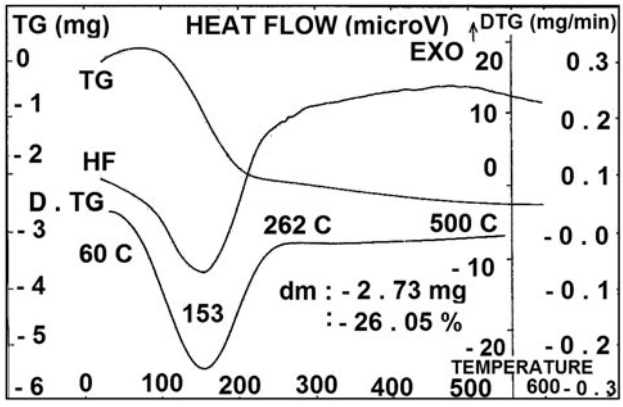

Fig. 8. Curves of TGA and DTA of the precipitated magnesium phosphate solid at $pH_0 = 8.6$.

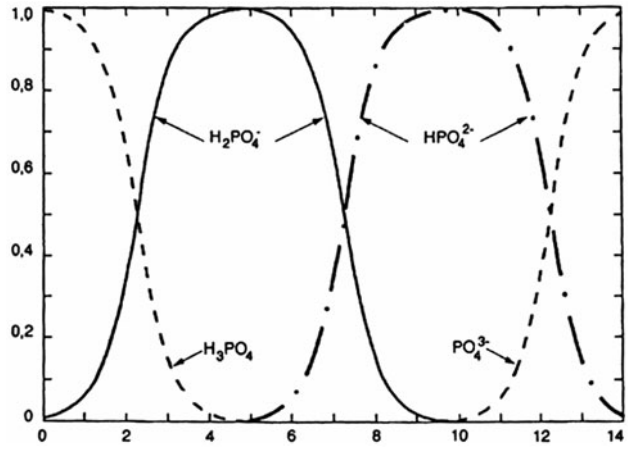

Fig. 9. Distribution diagram of phosphate species vs. pH [21].

xH_2O. In a comparative study of phosphate removal technologies using adsorption and fluidized bed crystallization process, Shun-Hsing and Yao-Hui obtained $CaHPO_4.2H_2O$ in the pH range 5.3–5.9 [25]. Fig. 9 represents the distribution diagram of phosphate species vs. pH [26], where pH_0 values HPO_4^{2-} was the predominant specie.

Ca/P at $pH_0 = 7$, 7.4, 7.8, 8.2 value ratio and 8.6 are on average of 1.44, below Ca/P value ratio of hydroxyapatite $Ca_{10}{\cdot}(PO_4)_6(OH)_2$ which is 1.67. However, these values were in conformity with some lacunar hydroxyapatites with a Ca/P ratio lower than 1.67 of formula $Ca_{10}\text{-}x(HPO_4)_x(PO_4)_{6\text{-}x}(OH)_{2-x}$ (without taking into account molecular water) [27]. Indeed, according to [28–30] lacunar compound would derive from the hydroxyapatite by the "substitution" of Ca^{2+} ions by the same number of H^+ ions and the elimination of OH^- ions to respect the electro neutrality, X varying from 0 to 2. For X = 2 is the octacalcic phosphate which presents a different crystallographic form with regard to hydroxyapatite [31–33]. According to Montel [34] amorphous $Ca_9(PO_4)_6$ forms first, then hydrolysis of $[PO_4^{3-}]$ ions occurs inside crystallites by forming HPO_4^{2-} ions in equal quantities. The HPO_4^{2-} ions substitute $[PO_4^{3-}]$ ions and OH^- ions which occupy the lacunar tricalcic calcium phosphate anion sites following the equation:

$$PO_4^3 + H_2O \rightarrow HPO_4^{2-} + OH^-$$

So that it corresponds to tricalcic calcium phosphate a series of solids represented by the formula:

$$Ca_9(PO_4)_{6-x}(HPO_4)_x(OH)_x \quad 0 \leq x \leq 1$$

For X = 1 it becomes $Ca_9\ (PO_4)_5(HPO_4)(OH)$ with Ca/P ratio of 9/6 which is the apatitic calcium phosphate.

3.3.1.2. Infra-red spectrometry. About the infra-red spectra of solid types: (a), (b) and (c), corresponding to the Ca/P ratio close to 1, absorption peaks appear at 3,540 and 3,488 cm^{-1} characteristics of valence vibrations of free H_2O (V_{H20}), at 3,290 and 3,161 cm^{-1} characteristics of valence vibrations of associated H_20 (V_{H20}) at 1,649 cm^{-1} characteristic of valence vibrations of H_20 of constitution (V_{H20}), at 1,220 and 790 cm^{-1} characteristics of bond elongation vibrations

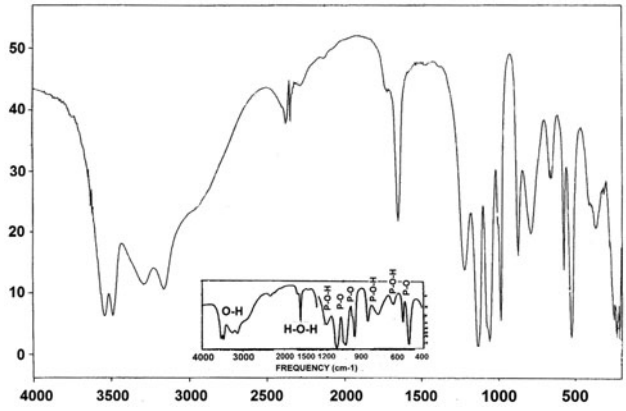

Fig. 10. The infra-red spectrum of solid type (a) and the infra-red spectrum of $CaHPO_4{\cdot}2H_2O$ obtained by Legeros [35].

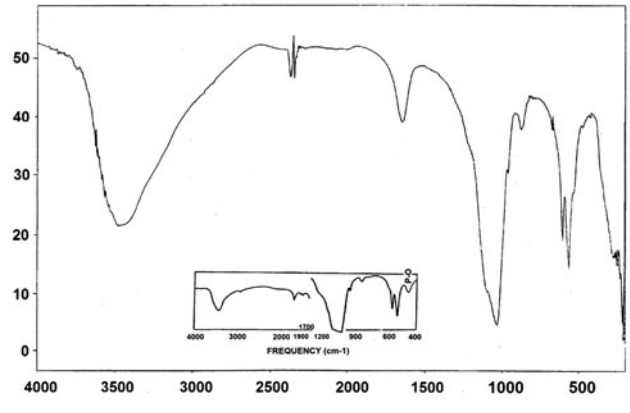

Fig. 11. The infra-red spectrum of solid type (d) and the infra-red spectrum of "OH-Apatite" obtained by Legeros [35].

$\delta_{P\text{-}O\text{-}H}$ at 1,135, 1,059 and 985 cm^{-1} characteristics of valence vibrations V_{PO} at 873 cm^{-1} characteristics of valence vibrations $V_{P\text{-}OH}$ and at 525 cm^{-1} characteristics of valence vibrations $V_{O\text{-}P\text{-}O}$. Fig. 10 shows the comparison between the infra-red spectrum of solid type (a) and the infra-red spectrum of $CaHPO_4{\cdot}2H_2O$ obtained by Legeros [35], Casciani and Condrate [36]. We can observe that the spectrum of solid type (a) is perfectly identical to infra-red spectrum of $CaHPO_4{\cdot}2H_2O$ with of those obtained by Legeros [35], Casciani and Condrate [36] and the characteristic bands are in conformity with those obtained by Casciani and Condrate [36].

About the infra-red spectra of solid types: (d), (e) and (f), corresponding to the Ca/P ratio close to 1,44, absorption peaks appear at 3,561 cm^{-1} characteristics of valence vibrations of V_{OH}^{-}, at 3,473 cm^{-1} characteristic of valence vibrations $V_{H\text{-}O\text{-}H}$ of free H_2O, at 2,367 cm^{-1} characteristic of valence vibrations $V_{O\text{-}H}$ of HPO_4^{2-} groups, at 1,647 cm^{-1} characteristic of valence vibrations $V_{H\text{-}O\text{-}H}$, at 1,112, 1,033 and 960 cm^{-1} characteristic of valence vibrations $V_PO_4^{3-}$, at 873 cm^{-1} characteristic of valence vibrations $V_{P\text{-}OH}$, at 602 and 562 cm^{-1} characteristics of elongation vibrations $\delta_{PO_4}^{3-}$. Fig. 11 shows the comparison between the infra-red spectrums of solid type (d) and the infra-red spectrum of "OH-Apatite", obtained by Legeros [35], Casciani and Condrate [36]. This spectrum is characteristic of hydroxyl apatite phosphate and it is identical to that obtained by Legeros [35], Casciani and Condrate [36].

The characteristic bands are in conformity of those obtained by Jaeger [27] of the followed precipitated solids:

N° 1	de Ca/P atom	1.33	$Ca_8(HPO_4)_2(PO_4)_4$
N° 2	de Ca/P atom	1.375	$Ca_{8.25}(HPO_4)_{1.75}(PO_4)_{4.25}(OH)_{0,25}$
N° 3	de Ca/P atom	1.42	$Ca_{8.5}(HPO_4)_{1.5}(PO_4)_{4.5}(OH)_{0.5}$
N° 4	de Ca/P atom	1.44	$Ca_{8.65}(HPO_4)_{1.,35}(PO_4)_{4.65}(OH)_{0.65}$
N° 5	de Ca/P atom	1.51	$Ca_{9.1}(HPO_4)_{0.9}(PO_4)_{5.1}(OH)_{1.1}$

and for the apatitic tricalcic phosphate $Ca_9(HPO_4)(PO_4)_5(OH)$ with Ca/P ratio 1.5.

3.3.1.3. X-ray diffraction. The X-ray diffraction diagrams of the precipitated solids at $pH_0 = 5.8$, 6.2 and 6.6 (Fig. 2 $pH_0 = 6.2$) present lines which we could index using ASTM card [21] of $CaHPO_4{\cdot}2H_2O$. The precipitates obtained at $pH_0 = 7$, 7.4 and 7.8 (Fig. 3 pH 7.8) is a crystallized product, although not visible on the diagram. Indeed, according to [22], if the drying of the product was carried out at 70°C, it crystallizes apatite, although the diagram is diffuse. Table 5 com-

Table 5
Crystallographic characteristics precipitated $CaHPO_4{\cdot}2H_2O$ compared to those of $CaHPO_4.2H_2O$ of ASTM [21] literature index card

	Precipitated product	Litterature			
D_{hkl}(A°)	7.56	7.56	4.24	3.05	7.57
I/I_1	100	100	100	75	100

D_{HKL}: Inter planer spacing between (hkl) Miller planes; I = transmitted light intensity; Io = incident light intensity; I/I_1: relative intensity.

pares D_{HKL} of the precipitated product pH 6.2 with those of $CaHPO_4{\cdot}2H_2O$ of the literature [21]. It was noted that those data are in conformity with ASTM [21] literature index card.

3.3.1.4. TGA and DTA. For the precipitated solid at $pH_0 = 6.2$ (Table 6), we observed three endothermic peaks. The first one at around 89°C corresponds to superficial water evaporation. The second peak beginning at 216 is characteristics of constitution water elimination. The last peak corresponds to the $CaHPO_4{\cdot}2H2O$ decomposition at 424°C [37].

For the precipitated solid at $pH_0 = 7.8$ (Table 7), we observed two peaks, one endothermic and the other exothermic. The first one at around 180°C corresponds to superficial water evaporation. The second peak exothermic at 354°C is due the phenomenon of crystallization [37]. Theoretical calculation of the percentage of $CaHPO_4{\cdot}xH_2O$ water liberated (Table 6).

Calculation:

The theoretical calculation of the percentage of $CaHPO_4{\cdot}xH_2O$ water gives:

$$\Delta M/M = 18x/(136 + 18x) \times 100$$

For x = 2:

$$\Delta M/M = 20.93\%$$

where M is the $CaHPO_4{\cdot}xH_2O$ molar mass, and ΔM the number of the mol of H_2O liberated. The value observed on graphic (Fig. 4) is about 20.46%, so very close of the theoretical value of 20.93, confirming that the precipitated solid is $CaHPO_4{\cdot}2H_2O$. The loss of mass of about 2.51% centred on 424°C is localized in a temperature where this reaction is possible.

$$2CaHPO_4 \leftrightarrow Ca_2P_2O_7 + H_2O$$

Theoretical calculation of the percentage of $CaHPO_4{\cdot}xH_2O$ water liberated (Table 7).

The proposed formula after IR spectra, RX difractogram and chemical analysis was of the type of $Ca_9\ (PO_4)_{6-x}\ (HPO_4)_x(OH)_x$ with $0 \leqslant x \leqslant 1$.

The theoretical calculation of the percentage of water of $Ca_9{\cdot}\ (PO_4)_{6-x}\ (HPO_4)_x(OH)_x$ gives:

$$\Delta M/M = 18x/(930 + 18x)$$

where M is the $Ca_9\ (PO_4)_{6-x}(HPO_4)_x(OH)_x$ molar mass and ΔM the mol number of H_2O liberated. The results are given in Table 8.

The experimental value of $\Delta M/M$ is 0.79%, corresponding to x = 0.4, where the theoretical value is

Table 8
Percentage of mass loss for x variant from 0 to 1

x	$\Delta M/M$
0	0
0.1	0.19
0.2	0.38
0.3	0.57
0.4	0.77
0.5	0.96
0.6	1.14
0.7	1.34
0.8	1.52
0.9	1.71
1.0	1.89

Table 6
Thermal analysis (TGA/DTA) of $CaHPO_4{\cdot}2H_2O$

Nature of the peak	Temperature (°C)	Loss of the mass $\Delta M/M$ (%)	Observations
Endothermic	89	3.40	Liberation of H_2O (humidity)
Endothermic	216	20.46	Liberation of H_2O (dehydration)
Endothermic	424	2.51	Decomposition of $CaHPO_4{\cdot}2H_2O$

Table 7
Thermal analyse (TGA/DTA) of $Ca_9\ (PO_4)_{5.6}(HPO_4)_{0.4}(OH)_{0.4}$

Nature of the peak	Temperature (°C)	Loss of the mass $\Delta M/M$ (%)	Observations
Endothermic	108	6.09	Liberation of H_2O (humidity)
Exothermic	354	0.78	Liberation of OH group

Table 9
Thermal analyse (TGA/DTA) of the precipitated magnesium phosphate

Nature of the peak	Temperature (°C)	Loss of the mass $\Delta M/M$ (%)	Observations
Endothermic	153	26.05	Liberation of H_2O (humidity)
Exothermic	354	0.78	Liberation of OH group and crystallization

0.77%. Consequently, the precipitated solid at $pH_0 = 7.8$ is $Ca_9(PO_4)_{5.6}(HPO_4)_{0.4}(OH)_{0.4}$.

3.3.2. Magnesium phosphates precipitation

3.3.2.1. Calculation of Mg/P ratio of precipitated solids by Chemical analysis. After magnesium phosphate precipitation, the treated solution was kept for a day before settling. Table 4 gives the chemical analysis of the precipitated solids. The minimal concentration of Mg^{2+} is reached for $[H_2PO_4^-]_0 = 12.8.10^{-3}$ mol/L and for one day settling time. This minimum was $1.20.10^{-4}$ mol/L = 2.916 mg/L.

Table 4 shows that the addition of $12.8.10^{-3}$ mol/L and $15.4.10^{-3}$ mol/L of $[H_2PO_4^-]_0$ produced the same Mg/P relation, therefore the same product. The precipitated solid is not controllable beyond the $15.4.10^{-3}$ mol/L concentration. Here, one can conclude that the product was without doubt magnesium phosphate.

3.3.2.2. Infra-red Spectrometry. The infra-red spectrum of the precipitated solids at $pH_0 = 8.6$ is represented in Fig. 6. The infra-red spectra of solid shows absorption peak at 3,404 cm^{-1} characteristic of valence vibrations of free H_2O V_{H2O}, at 2,364 cm^{-1} characteristic of valence vibrations $V_{O\text{-}H}$ of HPO_4^{2-} groups, at 1,645 cm^{-1} characteristic of valence vibrations of H_2O of constitution V_{H2O}, at 1,068 cm^{-1} characteristic of valence vibrations $V_P O_4^{3-}$, at 680 and 580 cm^{-1} characteristic of elongation vibrations $\delta_{PO_4}^{3-}$.

We can here conclude that our composite contains groups of HPO_4^{2-} and PO_4^{3-}.

3.3.2.3. X-ray diffraction. The X-ray diffraction of the precipitated solids at $pH_0 = 8.6$ is represented in Fig. 7. The results of X-ray diffraction of precipitated products show amorphous products.

3.3.2.4. TGA and DTA. For the TGA of the precipitated solid at $pH_0 = 8.6$ (Fig. 8), a loss of mass which is fast, from 60 to 262°C, centred on 153°C is observed. It is an endothermic reaction, probably a dehydration of hydrated precipitated magnesium phosphate. About 20.46% loss of mass are observed (Table 9).

4. Conclusion

The paper was centred on calcium phosphates precipitation through synthetic hard water softening by monosodium phosphate. The effect of the initial pH, Ca, Mg and PO_4 concentrations in calcium phosphates precipitation was reported. We can conclude from the experimental results that:

(1) The variation of pH_0 due to the addition of NaOH solution allowed the precipitation of $CaHPO_4.2H_2O$ from pH_0 5 to 6.6 and lacunar apatite $Ca_9(PO_4)_{6-x}(HPO_4)_x(OH)_x$ from pH_0 7 to 8.6.
(2) The amorphous acid phosphates of magnesium are obtained at $pH_0 = 8.6$.
(3) The precipitated calcium phosphates are of high purity.

This addition of calcium salts can be used to remove phosphate from wastewater, where phosphorus will be recovered as calcium phosphates and used as soluble fertilizer in agriculture. Moreover, pure precipitated calcium phosphates can be used in nanotechnology where they undergo laser ablation to obtain nanoparticles that could be used in biomedical technology to fill cracks responsible of tooth enamel pain. The use of calcium phosphate nanoparticles in tooth enamel accelerates recovery ten times more rapidly than the use of calcium phosphates monoparticles (apatite). The nanoparticles simulate the tooth natural matter and the composite remineralized layer conveniently acts as a natural one.

References

[1] J. L. Potelon, K. Zysman, Le guide des analyses de l'eau potable [The Guide of Clean Water Analyses], Edition, La Lettre du Cadre Territorial [The Letter of Territorial Framework], Voiron, France, 1998.
[2] WHO, Guidelines for drinking-water quality, third edition, Vol. 1, Recommendation, Geneva, 2004.

[3] H. Roques, Fondements théoriques du traitement chimique des eaux (Theoretical basis of chemical waters treatment), Vol I, Ed Technique et documentation (Documentation and technic), Paris, 1990.
[4] GLS, L'élimination du phosphore présent dans les eaux résiduaires urbaines (Phosphorus elimination in urban residuaries waters), Memotec no 23, 2003.
[5] CEMAGREF, Traitement du phosphore dans les petites stations d'épuration à boues activées, Document technique, FNDAE no 29, France, 2004.
[6] E.C. Moreno, W.E. Brown, G. Osborn, Solubility of dicalcium phosphate dehydrate in aqueous systems, Soil Sci. Soc. Am. Proc. 24 (1960) 94–98; Stability of dicalcium phosphate dehydrate in aqueous solutions and solubility of octacalcium phosphate, ibid. 24 (1960) 99–104.
[7] W.E. Brown, N. Eidelman, B. Tomazic, Octacalcium phosphate as a precursor in biomineral formation, Adv. Dent. Res. 1 (1987) 306–313.
[8] E.C. Moreno, K. Varughese, Crystal growth of calcium apatites from dilute solutions, J. Crystal Growth 53 (1981) 20–30.
[9] P. Koutsoukos, Z. Amjad, M.B. Tomson, G.H. Nancollas, Crystallization of calcium phosphates: A constant composition study, J. Amer. Chem. Soc. 102(5) (1980) 1553–1557.
[10] G.H. Nancollas, S. Mann, J. Webb, R.J.P. Williams (Eds), Bio mineralization, VCH, New York, pp. 157–187, 1989.
[11] P.T. Cheng, Octacalcium phosphate formation *in vitro*: Implications for bone formation, Calcif. Tissue Int. 37 (1985) 91–94.
[12] J. Christoffersen, M.R. Christoffersen, W. Kibalczyc, F.A. Andersen, A contribution to the understanding of the formation of calcium phosphates, J. Cryst. Growth 94 (1989) 767–777.
[13] S. Mandel, A. Cuneyt Tas, Brushite ($CaHPO_4{\cdot}2H_2O$) to octacalcium phosphate ($Ca_8(HPO_4)2(PO_4)4{\cdot}5H_2O$) transformation in DMEM solutions at 36.5˚C, Mater. Sci. Eng. C 30 (2010) 245–254.
[14] H.E.L. Madsen, Heterogeneous nucleation of calcium phosphates I: Kinetics of nucleation of tetracalcium monohydrogen phosphate on crystals of calcium monohydrogen phosphate dehydrate, Acta Chem. Scand. 24 (1970) 1677–1686.
[15] B.B. Tomazic, M.S. Tung, T.M. Gregory, W.E. Brown, Mechanism of hydrolysis of octacalcium phosphate, Scanning Microsc. 3 (1989) 119–127.
[16] G.H. Nancollas, B. Tomazic, Growth of calcium phosphate on hydroxyapatite crystals: Effect of supersaturation and ionic medium, J. Phys. Chem. 78 (1974) 2218–2225.
[17] G.H. Nancollas, J.S. Wefel, Seeded growth of calcium phosphates: Effect of different calcium phosphate seed materials, J. Dent. Res. 55 (1976) 617–624.
[18] M. Boutinguiza, R. Comesaña, F. Lusquiños, A. Riveiro, J. Pou, Production of nanoparticles from natural hydroxylapatite by laser ablation, Nanoscale Res. Lett. 6 (2011) 255–259.
[19] M. Boutinguiza, J. Pou, F. Lusquiños, R. Comesaña, A. Riveiro, Laser-assisted production of tricalcium phosphate nanoparticles from biological and synthetic hydroxyapatite in aqueous medium, Appl. Surf. Sci. 257(12) (2011) 5195–5199.
[20] C. Calvo, R. Gopal, The structure of whitlockite from the Palermo Quary, J. Amer. Mineralogy 60 (1975) 120–133.
[21] ASTM literature index card N˚ 9–77.
[22] M.K. Domontovich, O.V. Sarubina, Determination of solubility product of dicalcium phosphate, Biochem. Z. (1925) 464 clxiii.
[23] T.M. Gregory, E.C. Moreno, W.E. Brown, Solubility of CaHPO4.2H2O in the system Ca(OH)2–H3PO4-H2O at 5, 15 et 37,5˚C, J. Res. Natl Bureau Stand. 74A (1970) 461–475.
[24] P. Molle, Filtres plantés de roseaux: Limites hydrauliques et rétention du phosphore (Reeds plantes filters: Hydraulics limitations and phosphorus retention), Thèse de doctorat (Doctorate thesis), Montpellier, Université de Montpellier II (University of Montpellier II), 2003, p. 267.
[25] Y.-H. Huang, Y.-J. Shih, C.-C. Chang, S.-H. Chuang, A comparative study of phosphate removal technologies using adsorption and fluidized bed crystallization process, Desalin. Water Treat. 32 (2011) 351–356.
[26] G. Demns, M. Hays, M. Hielije, Chemical Separation and Measurements, Sounders Golden Sunburst Series, Philadelphia, PA, 1974.
[27] C. Jaeger, S. Maltsev, A. Karrasch, Progress of structural elucidation of amorphous calcium phosphate (ACP) and hydroxyapatite (HAp): Disorder and surfaces as seen by solid state NMR, Key Eng Mater 309–311 (2006) 69–72.
[28] L. WINAND, Thèse de doctorat (Doctorate thesis), Université de Liège (University of Liege), 1960.
[29] L. Winand, Etude physico-chimique du phosphate trical-cique hydrate et de l'hydroxylapatite (Physico-chemical study of hydrated tricalcium phosphate and hydroxyapatite), Chem. Ann. 13(6) (1961) 941–967.
[30] S.V. Dorozhkin, Calcium orthophosphates occurrence, properties, biomineralization, pathological calcification and biomimetic applications, Biomatter 1(2) (2011) 121–164.
[31] W.E. Brown, J.P. Smith, J.R. Lehr, A.W. Frazier, Octacalcium phosphate and hydroxyapatite, Nature 196 (1962) 1048–1055.
[32] K. Onuma, Recent research on pseudobiological hydroxyapatite crystal growth and phase transition mechanism, Prog. Cryst. Growth Charact. Mater. 52 (2006) 223–245.
[33] J.C. Elliott, Structure and Chemistry of the Apatites and Other Calcium Orthophosphates, Studies in Inorganic Chemistry 18, Elsevier, 1994.
[34] G. Montel, G. Bonel, J. C. Trombe, J. C. Heughebaert et C. Rey, 1er congrès international des composes phosphorés (First international congress of combined phosphorus), Rabat, 17–21 Oct. 1977.
[35] R.Z. Legeros, D. Lee, G. Quirolgico, W.P. Shirro and Reich, In vitro formation of Dicalcium Phosphate Dihydrate CaHPO4.2H2O, Scanning Electron Microscopy, 1983, pp. 407–418.
[36] F.S. Casciani and R.A. Condrate Sr., The infrared and Raman Spectra of Several Calcium Hydrogen Phosphates, Proc. 2nd Internatl., Congress on Phosphorus compounds. Boston, 1980, pp. 175–190.
[37] J.P. Maity, L. Tz-Jiun, C.H. Pai-Heng, C. Chien-Yen, A.S. Reddy, S.B. Atla, C. Young-Fo, C. Hau-Ren, C. Chien-Cheng, Synthesis of Brushite Particles in Reverse Microemulsions of the Biosurfactant Surfactin, Int. J. Mol. Sci. 12 (2011) 3821–3830.